

Wing Warping Control of Flexible Membrane Wing Under Gusty Conditions

S. Lee ¹, T. Tjahjowidodo ¹, H.C. Lee ²

¹ School of Mechanical and Aerospace Engineering, Nanyang Technological University, Singapore
e-mail: TTEGOEH@ntu.edu.sg

² Dept. of Mechanical and Manufacturing Engineering, University of Calgary, 2500 University Drive N.W. Calgary, T2N 1N4, Canada

Abstract

Flying in gusty winds with a mini-UAV has always been a challenge as the moment of inertia and weight of the vehicle is typically low. In order to improve the flight quality of the mini-UAV, a flexible membrane wing has been fabricated with added desirable features. This wing is able to dampen the high-frequency gusts via the adaptive washout and also fold along the fuselage for quick storage and deployment. However, the actuation of the wing for roll control is difficult if these two properties are not to be compromised. A novel method of wing warping for roll control with a tendon-sheath has been investigated. The nonlinearities of the tendon-sheath mechanism require extra control strategies for accurate wing warping control. The nonlinear characteristics of the wing warping via tendon-sheath has been examined, and a suitable model is designed and implemented in a controller to compensate for the nonlinearity. The performance and robustness of the system is subsequently tested in gusty conditioned wind tunnel with satisfactory results.

1 Introduction

Mini-UAV is a piece of useful equipment in many situations. Loosely defined as a UAV small and light enough for a person to operate, mini-UAVs have been used in various scenarios such as border surveillance and real-time observation of a battlefield. There are many advantages of the mini-UAV such as stealthy (low heat signature, low radar signature, low operating noise and also very difficult to visually detect while operating in the sky), economical and safe, however there are a few very critical flaws in regards to the mini-UAV which prevents these machines from being deployed in large scale.

The two main drawbacks of the conventional mini-UAV are difficult to store and also difficult to operate in gusty weather conditions. Typically, a mini-UAV will require up to 1 meter of wingspan, resulting in a need of dismantling the aircraft for storage and transportation, and then reassembling it at the site to execute the mission. Such work of disassembling and reassembling of the mini-UAV prohibits the operator from deploying the aircraft immediately at the mission site, as it takes some time and also some effort to assemble the mini-UAV. This is costly in terms of the time wasted, as the target of surveillance may have left the operational zone and therefore reducing the effectiveness of the mini-UAV mission. Besides, human errors during assembly, as well as foreign objects such as sand or dust, may enter the mini-UAV while the assembly is in the process.

Furthermore, due to the small moment of inertia and light weight, the mini-UAVs are very susceptible to bad weather conditions. Gusty environments, such as mountainous areas and the seas are very challenging locations for a mini-UAV to handle. Typically, an on-board autopilot with various sensors and a stabilization augmentation system (SAS) will be working very intensively in order to stabilize the mini-UAV. In some cases, the actuators themselves are overpowered by the gust disturbance, therefore rendering bad quality

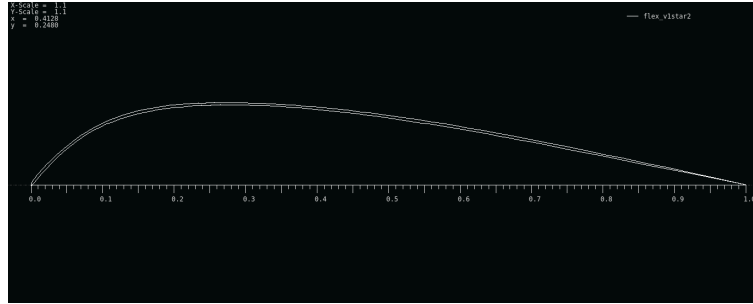


Figure 1: The airfoil of the FMW.

surveillance footage due to the vibrations of the camera mounted on the fuselage during the mission. The aircraft will be difficult to operate and will also have less efficient flight quality.

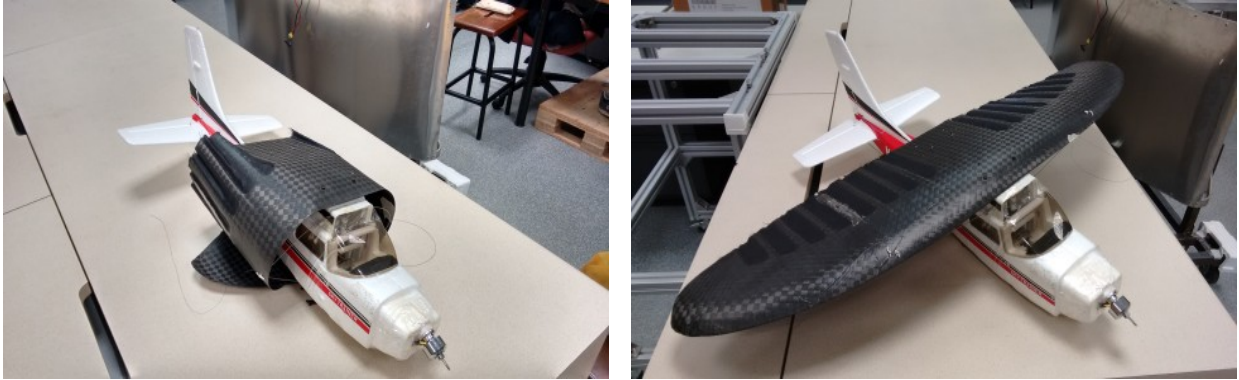
In order to tackle the problems mentioned above, Ifju et al. [1] have devised an innovative flexible membrane wing (FMW) which can be folded around the fuselage for storage inside a tube for transportation and quick deployment, and also incorporates an adaptive washout mechanism to dampen the gusty airflow during flight. However, the FMW has no control surface, or rather, it is impossible to install control surfaces i.e. ailerons which give the rolling moment for the mini-UAV. To compensate for that, rudders were used instead to induce rolling moment, which will be insufficient. A new method of actuating the FMW via tendon-sheath mechanism (TSM) to warp the FMW was introduced [2], creating ample rolling moment for the aircraft. TSM induced wing warping can create rolling moment without compromising on the two main advantages of the FMW, which are being foldable and being able to dampen the gusty airflow via adaptive washout mechanism.

This paper examines the robustness of the wing warping control via TSM under gusty conditions. Experiments were held to generate artificial gusty airflow, and the FMW was actuated in the artificial gusty airflow with random inputs. The experimental results were compared with the results from the controlled environment without disturbances. Section 2 discusses the unique properties of the FMW and also the wing warping actuation methods suitable for FMW. In Section 3 the nonlinear properties of the TSM are discussed and the representative math model is presented. Section 4 presents the control strategy for the TSM actuated wing warping. The experimental setup and the actuation methods are also discussed in this section. The simulation regarding the design of a suitable gusty environment for the FMW is discussed in Section 5. The computation fluid dynamics (CFD) results are shown in this section. The implementation of the control strategy in a designed gusty environment, and also the adaptive washout mechanism validation is shown in Section 6. The results and discussion of the experiment are followed in Section 7.

2 Flexible Membrane Wing & Wing Warping

The FMW is fabricated by layering pre-preg carbon fiber and Nylon cloth onto a mold and then cured in an autoclave. The resulting FMW is very durable, and also flexible enough to fold downwards around the fuselage for storage, as shown in Figure 2a. The unique airfoil shape makes it difficult to fold upwards, therefore providing enough strength to resist the aerodynamic loads without buckling. The airfoil of the FMW thin and cambered, as shown in Figure 1. The unique shape of this airfoil and the low thickness of the wing allow for the folding mechanism to work well. The FMW has a wingspan of 1 meter, has an area of 0.19 square meters, and only weighs 160 grams with 1.2 mm thickness. It can generate up to 35 N of lift without buckling during wind tunnel tests, which is a feat given the low weight of the FMW.

Another unique property of the FMW is the ability to reject and dampen gusts via the adaptive washout mechanism. The FMW is both chord-wise and span-wise flexible, with the chord-wise flexibility allowing it to change the wing airfoil shape to adapt to the disturbances such as gusts. For example, as the gust attacks



(a) Flexible membrane wing in the folded state.

(b) Flexible membrane wing unfolded.

Figure 2: Flexible membrane wing in both folded and normal state.

from below the wing, the FMW will warp according to the direction of the gust, decreasing the effective angle-of-attack of the FMW, therefore, dampen the change in aerodynamic forces exerted by the gusts [1]. The FMW will also adapt according to the headwind velocity, and changing its shape to increase or decrease the aerodynamic forces to provide a better flight quality and higher stall resistance.

One alternative method to provide the rolling moment for the FMW is to warp the wings, as control surfaces such as ailerons are impossible to be installed on the FMW due to the lack of space and thickness to house the aileron. Wing warping has been practiced since the first human flight [3], and for the Wright brothers pulleys and tethers were used. For the FMW, various methods were used such as Kevlar strings and torque rods [4, 5]. The drawback of Kevlar string is that they break easily and the torque rod hinders the folding of the FMW for storage. In this paper, the actuation method is via TSM, which can provide enough rolling moment while still allowing the FMW to fold and not hinder the adaptive washout phenomenon.

3 Tendon-Sheath Characteristics & Modeling

A TSM functions by transmitting the tension forces from one end to the other. Figure 3a shows the schematic of the tendon-sheath, where a flexible sheath encloses a low friction, Teflon-coated Kevlar wire which is the tendon. Due to the friction between the tendon and the sheath, as well as backlash [6], the TSM exhibits nonlinear behaviors, which is referred to as hysteresis [7–10]. There are four main phases during the transmission of tension, as shown in 3b. Initially, the tension forces are not transmitted in Phase 1 due to the backlash and also friction between the tendon and the sheath. After enough tension force has been given, the TSM continues to Phase 2, where the P_{out} increases with P_{in} . Phase 3 is the opposite of Phase 1, where the tension forces have to be reduced enough in order to overcome the backlash and friction of the tendon-sheath, therefore, no translation of position is detected in Phase 3. In Phase 4, the P_{out} will decrease together with P_{in} . This unique characteristic of the tendon-sheath is attributed to the friction force occurring between the tendon and the sheath that exhibits nonlocal memory behavior [11, 12].

The hysteresis behavior of the TSM induced wing warping is best modeled with the General Bouc-Wen equation [13], which is used in this paper. The hysteresis model of the TSM actuated wing warping is expressed as:

$$\begin{aligned}\theta(x)(t) &= \alpha_1 x^2 + \alpha_2 x + \alpha_3 + \alpha_z z \\ \dot{z} &= \dot{x}[A - |z|^n \Psi(x, \dot{x}, z)] \\ \Psi(x, \dot{x}, z) &= \beta \phi^T\end{aligned}$$

where β and ϕ are matrices given as:

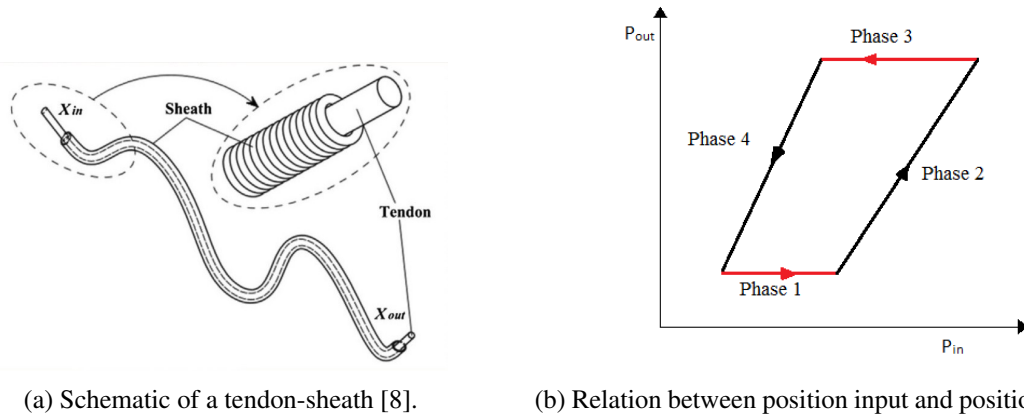


Figure 3: Tendon-sheath and its hysteresis characteristics.

$$\beta = [\beta_1 \beta_2 \beta_3 \beta_4 \beta_5 \beta_6]$$

$$\phi = [\text{sgn}(\dot{x}z) \text{sgn}(x\dot{x}) \text{sgn}(xz) \text{sgn}(\dot{x}) \text{sgn}(z) \text{sgn}(x)]$$

A total of 12 parameters is to be optimized in order to identify the model for the TSM actuated wing warping hysteresis. The optimized parameters used for control design are shown in 1. Further information on the identification and optimization procedures can be found in [2].

$$\begin{aligned} \beta &= [19.8351 \quad -8.6135 \quad 0.8325 \quad -3.1266 \quad 10.6984 \quad -18.5] \\ A &= 3.9953 \\ n &= 3.1179 \\ \alpha &= [-0.0205 \quad 0.7120 \quad 0.7958] \\ \alpha_z &= 0.5369 \end{aligned} \tag{1}$$

with the RMS error being 0.26° .

4 Wing Warping Control Implementation

Due to the high degree of nonlinearity of the wing warping system, a robust control strategy is necessary to accurately control the position of the wing warping. Feedback control alone, i.e. PID controller is not sufficient as the nonlinearity is very severe. A feed-forward controller was designed based on the General Bouc-Wen model of the FMW warping via TSM found in the previous chapter. With an accurate model of the nonlinear system, the wing warping control is much more robust and exact. The feed-forward controller is coupled to a feedback controller, resulting in a control algorithm as shown in Figure 4. This technique is presented in [14] that was implemented also on a system with nonlocal memory hysteresis.

The details regarding the experimental setup for FMW warping via TSM can be found in [2]. Random inputs were generated via dSPACE, with the control algorithm designed with Matlab Simulink and integrated to dSPACE.

5 Design of the Gusty Environment via CFD Simulation

A CFD simulation was done to assess the incoming flow from the wind tunnel. An obstacle with the size of 60 x 200 x 100 mm was placed in a test section with a dimension of 780 x 720 x 2000 mm and the inlet flow

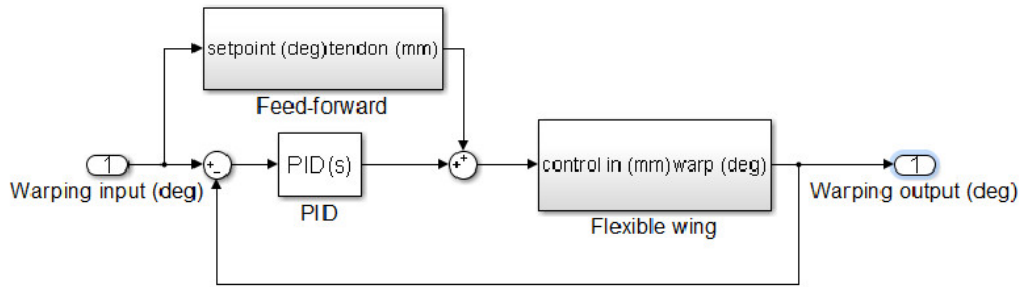
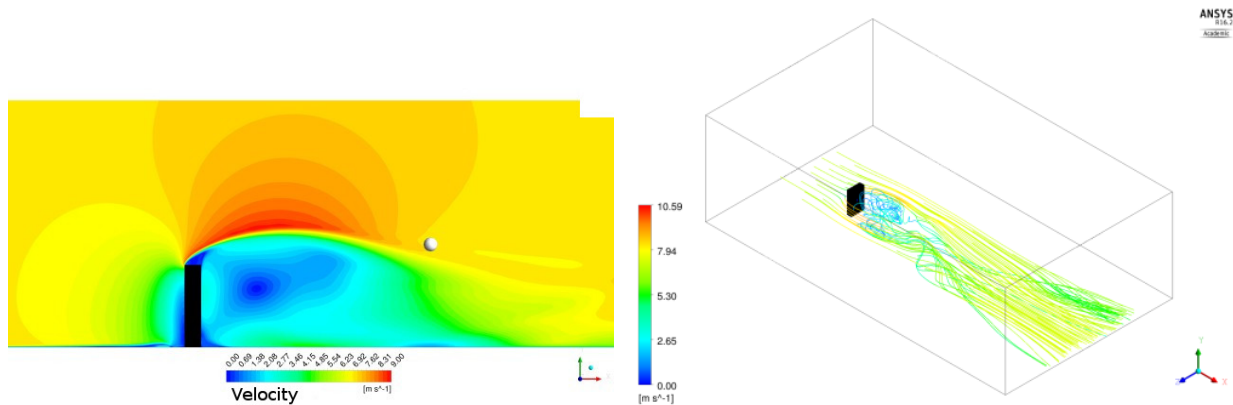


Figure 4: Control strategy of the FMW warping via TSM.



(a) Three dimensional velocity profile of the solid obstacle. (b) Velocity vectors of the wind around the obstacle.

velocity was set to be 7 m/s to find out where is the suitable location for placing the FMW in order to get the gusty airflow. Figures 5a and 5b illustrates the velocity profile of the airflow after being perturbed by the solid obstacle.

The instantaneous vortex cores generated by the bluff body, which is placed in the vicinity of ground, is illustrated in Figure 6. By comparing the two frames, it can be observed how the vortex is detached and shed downstream, introducing perturbation at a frequency of approximately 110 Hz to the flow. As the turbulence value from the CFD simulation is many degrees higher than the usual values found in a standard atmospheric condition, the artificial gusty environment is therefore much more severe than the real environment. The desired location for the FMW during the wind tunnel test is indicated by a blue sphere in the figure.

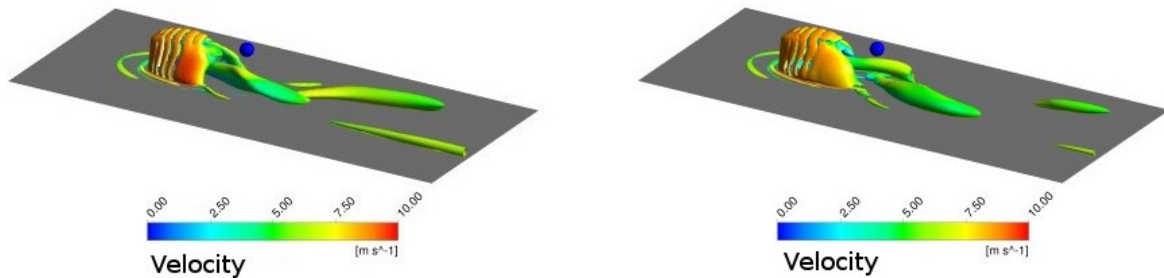
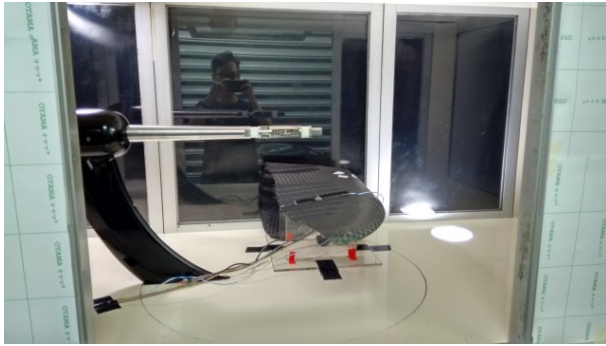


Figure 6: Vortex structure identified using Q-criterion ($Q = 10,000$). The Q-criterion is colored with velocity magnitude.



(a) The left side of the FMW is folded to fit inside the wind tunnel during experiment.



(b) Gust generator, capable of oscillating up to 7 Hz.

6 Experimental Setup

There are two separate wind tunnel tests presented in this paper. The first wind tunnel experiment will be the gusty wind tunnel setup to test the TSM actuated FMW warping, and the second wind tunnel experiment is carried out to validate the adaptive washout mechanism.

6.1 Robustness Test

With the available design of the gusty environment, the whole experimental setup was replicated following the design in the test section of a closed loop wind tunnel, with 780 mm in width, 720 mm in height and 2000 mm in length. Due to the space constraint of the test section, the left side of the FMW was folded, and only the right side of the FMW was fitted with the flex sensor and TSM to be tested in the gusty air flow, as shown in Figure 7a. Following the design, the experiment was done at 7 m/s wind speed. By observation, the FMW was oscillating vigorously during the whole experiment, proving that a turbulent flow was indeed present at the location of the FMW, coinciding with the CFD simulation results. The experiment was performed at 12 m/s wind speed as well, to further verify the robustness of the controller in different wind speeds. Similarly, the FMW was oscillating as well in 12 m/s winds.

6.2 Adaptive Washout Validation

The fundamental frequency of the FMW is desired because the FMW is to be placed in a gusty environment with that specific frequency, to acquire the gust response in the worst case scenario. To study the natural frequencies of the FMW, a modal testing was performed. A load cell was attached to the trailing edge of the FMW, and the leading edge was struck with the impact hammer. The fundamental frequency of the FMW is found to be 7 Hz from the FRF.

With the fundamental frequency result, another wind tunnel test was carried out to validate the adaptive washout mechanism of the FMW. The wind tunnel used for this experiment is a low-speed wind tunnel, with a test section of 2.3 meters wide, 1.5 meters high and 6 meters long. The FMW has a wingspan of close to 1 meter, therefore, a huge test section such as this wind tunnel is desired for more accurate results. A gust generator, as shown in Figure 7b is used to generate oscillatory gust in the longitudinal direction. The gust generator was designed and built to generate oscillations up to 7 Hz, as the fundamental frequency of the FMW in the chord-wise direction was determined to be 7 Hz via the modal testing. The gust generator is placed inside the wind tunnel test section, before the model as illustrated in Figures 8a & 8b.

The FMW performed much better in the gusty airflow when compared to the rigid wing. Lift and drag force values were recorded for both the FMW and rigid wing model. From the data, the variance of the lift force experienced by the FMW model is 0.010 and the variance of the drag force is 0.042, as compared to a



(a) Flexible membrane wing under gusty airflow in wind tunnel. (b) Rigid aluminum wing under gusty airflow in wind tunnel.

Figure 8: Wind tunnel setup with gust generator before the model. Oscillating gusts with various frequencies are produced and the gust response of the models are recorded.

variance of 0.047 and 0.067 respectively for the rigid wing model. As the FMW is flexible in the chord-wise direction, the adaptive washout mechanism helps to alleviate the aerodynamic forces induced by the gusty airflow. This experiment has shown that the adaptive washout mechanism still functions well even with the TSM attached to the FMW.

7 Results and Discussion

Figure 9 shows the results of the experiment with the wind speed at 7 m/s, while Figure 10 shows the results with the wind speed at 12 m/s. It can be observed from the plots that the controller works well in both wind speeds, demonstrating robustness in noisy and gusty conditions. The output of the wing warping has a much better performance with the controller when compared with the open loop, as shown in Figures 9a and 10a. From the results, it can be concluded that FMW warping via TSM can be done accurately with the designed control strategy, without compromising on the two desirable properties of the FMW, which are foldable around the fuselage as well as the adaptive washout mechanism. The results from the experiment have shown that the wing warping control algorithm performs efficiently even when there are huge amounts of disturbances introduced to the system, further proving the robustness of the controller. The feed-forward coupled with feedback controller results in a superior performance compared to the open loop system. The future continuation of this work will be to further enhance the control algorithm to include a feedback for the rolling moment control with wing warping via TSM.

Acknowledgments

The authors would like to thank Final Year Project student Benedict Lai Chen Kin for his assistance in this experiment.

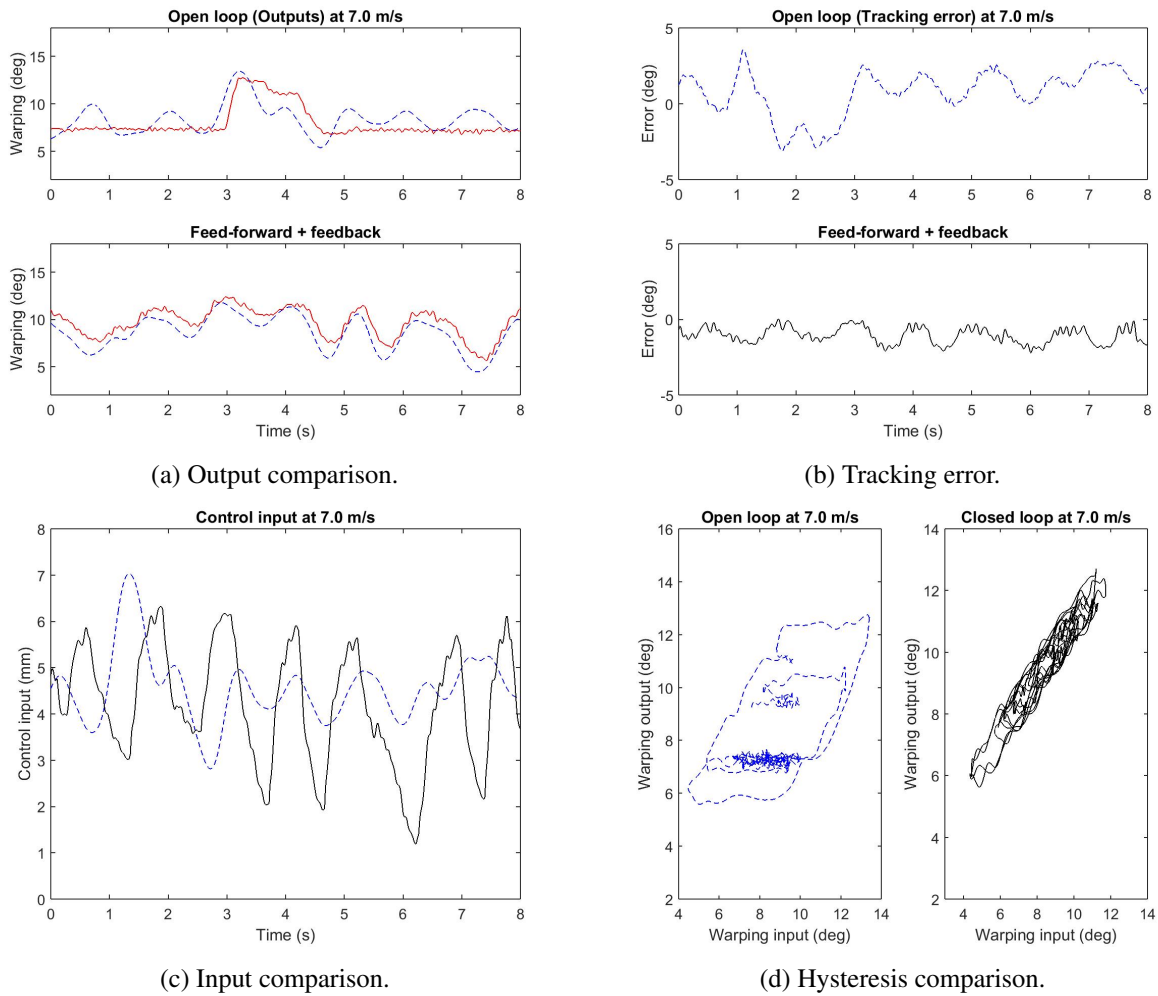


Figure 9: Controller performances of the wing warping with tendon-sheath actuation under gusty environments, with wind speed of 7 m/s. For the output comparison, the setpoint is in dashed blue, while the output is in red. For others the open loop is dashed blue, feed-forward plus feedback is in black.

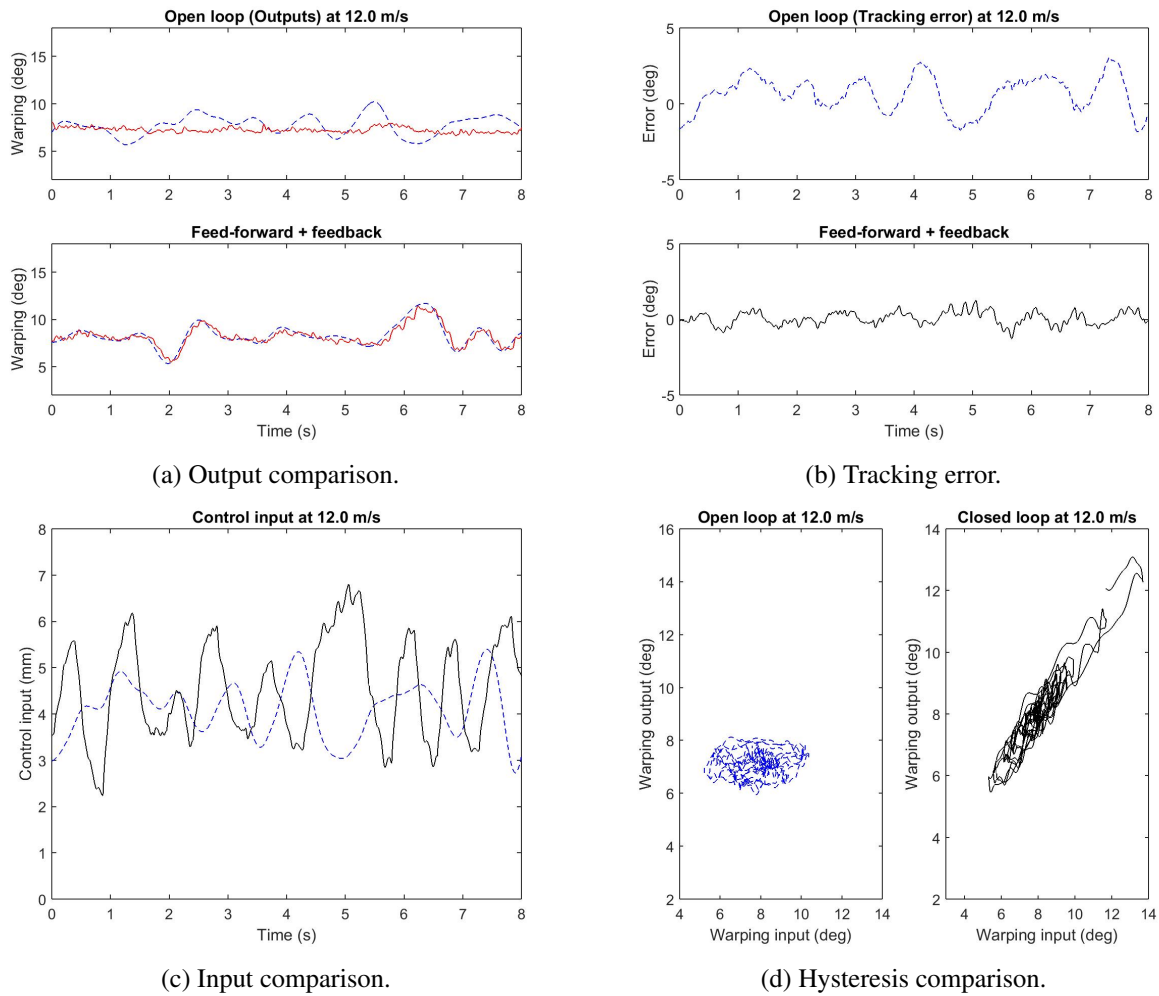


Figure 10: Controller performances of the wing warping with tendon-sheath actuation under gusty environments, with wind speed of 12 m/s. For the output comparison, the setpoint is in dashed blue, while the output is in red. For others the open loop is dashed blue, feed-forward plus feedback is in black.

References

- [1] P. Ifju, D. Jenkins, S. Ettinger, Y. Lian, W. Shyy, and M. Waszak, *Flexible-wing-based micro air vehicles*, ser. *Aerospace Sciences Meetings*. American Institute of Aeronautics and Astronautics, 2002, doi:10.2514/6.2002-705.
- [2] S. Lee, T. Tjahjowidodo, and S. K. Moon, *Flexible membrane wing warping using tendon-sheath mechanism*, in *Control and Automation (MED), 2015 23th Mediterranean Conference on*, June 2015, pp. 624–629.
- [3] C. Culick F. E., *The Wright Brothers: First Aeronautical Engineers and Test Pilots*, AIAA Journal, vol. 41, no. 6, pp. 985–1006, 2003, doi: 10.2514/2.2046.
- [4] H. Garcia, M. Abdulrahim, and R. Lind, *Roll Control for a Micro Air Vehicle Using Active Wing Morphing*, ser. *Guidance, Navigation, and Control and Co-located Conferences*. American Institute of Aeronautics and Astronautics, 2003, doi:10.2514/6.2003-5347.
- [5] M. Abdulrahim, H. Garcia, and R. Lind, *Flight Testing a Micro Air Vehicle Using Morphing for Aeroelastic Control*, ser. *Structures, Structural Dynamics, and Materials and Co-located Conferences*. American Institute of Aeronautics and Astronautics, 2004, doi:10.2514/6.2004-1674.
- [6] T. Tjahjowidodo, F. Al-Bender, and H. Van Brussel, *Experimental Dynamic Identification of Backlash Using Skeleton Methods*, *Mechanical Systems and Signal Processing*, vol. 21, no. 2, pp. 959–972, 2007.
- [7] T. Do, T. Tjahjowidodo, M. W. S. Lau, and S. J. Phee, *An investigation of friction-based tendon sheath model appropriate for control purposes*, *Mechanical Systems and Signal Processing*, vol. 42, no. 1, pp. 97–114, 2014.
- [8] T. Do, T. Tjahjowidodo, M. Lau, T. Yamamoto, and S. Phee, *Hysteresis modeling and position control of tendon-sheath mechanism in flexible endoscopic systems*, *Mechatronics*, vol. 24, no. 1, pp. 12–22, 2014.
- [9] T. V. Minh, T. Tjahjowidodo, H. Ramon and H. Van Brussel, *Non-local Memory Hysteresis in A Pneumatic Artificial Muscle (PAM)*, in *Control and Automation (MED), 2009 17th Mediterranean Conference on*, June 2009, pp. 640–645.
- [10] V. Hassani and T. Tjahjowidodo, *Structural Response Investigation of A Triangular-based Piezoelectric Drive Mechanism to Hysteresis Effect of the Piezoelectric Actuator*, *Mechanical Systems and Signal Processing*, vol. 36, no. 1, pp. 210–223, 2013.
- [11] T. Tjahjowidodo, *Theoretical analysis of the dynamic behavior of presliding rolling friction via skeleton technique*, *Mechanical Systems and Signal Processing*, vol. 29, pp. 296–309, 2012.
- [12] V. Hassani, T. Tjahjowidodo, and T. N. Do, *A survey on hysteresis modeling, identification and control*, *Mechanical systems and signal processing*, vol. 49, no. 1, pp. 209–233, 2014.
- [13] J. Song and A. Der Kiureghian, *Generalized Bouc–Wen model for highly asymmetric hysteresis*, *Journal of engineering mechanics*, vol. 132, no. 6, pp. 610–618, 2006.
- [14] T. V. Minh, T. Tjahjowidodo, H. Ramon and H. Van Brussel, *Control of a Pneumatic Artificial Muscle (PAM) with Model-Based Hysteresis Compensation*, in *Advanced Intelligent Mechatronics (AIM), 2009 IEEE/ASME International Conference on*, July 2009, pp. 1082–1087.